Band structure and related properties of molybdenum

A. R. Jani,* G. S. Tripathi,† N. E. Brener, and J. Callaway
Department of Physics and Astronomy, Louisiana State University, Baton Rouge, Louisiana 70803-4001
(Received 24 October 1988)

Self-consistent, all-electron, local-density calculations are reported for bcc molybdenum, using the linear combination of Gaussian orbitals (LCGO) method. We obtain the density of states, the Fermi surface, charge form factors, the Compton profile, and the optical conductivity. Results are compared with other calculations and with experiments where these exist. A possible ferromagnetic state is found for an increased lattice constant, developing at about 8.07 a.u.

I. INTRODUCTION

This is the third in a series of papers concerning the electronic structure of cubic 4*d* transition metals. Our previous calculations have considered rhodium[1] and niobium.[2] In this paper, we report an all-electron self-consistent calculation of energy bands and related properties of bcc molybdenum based on the local-density approximation in density functional theory and employing the linear combination of Gaussian orbitals (LCGO) method.[3]

The electronic structure of molybdenum is characterized, as is the case for 3*d*, 4*d*, and 5*d* metals in general, by the overlap and hybridization of a wide nearly free-electron *s-p* band with a relatively narrower *d*-band complex. This leads normally to a rather complex Fermi surface of several sheets. In the case of molybdenum, the Fermi energy falls in a range of energies in which the *d*-electron density of states is not large, leading to a low-electron specific heat, comparable to that typically found in simple metals, or noble metals.[4]

Non-self-consistent band calculations for molybdenum are described in Refs. 5–11. Previous self-consistent band calculations on Mo include the work of Alperovich *et al.*,[12] who employed the Green's-function method and used the calculation to interpret x-ray emission bands. Moruzzi *et al.*[13] performed a self-consistent band calculation of Mo using the Korringa-Kohn-Rostoker (KKR) method in which the electron charge density was assumed to be of the muffin-tin form. They computed the density of states and the radial charge density and compared the latter with that obtained for the Mo atom. Zunger *et al.*[14] carried out a self-consistent band calculation using a nonlocal-pseudopotential approach and mixed-basis representation for the crystalline wave functions. Fermi-surface cross sections and the density of states were computed and the spatial variation of the charge density associated with several band states was discussed. Bacalis *et al.*[15] performed band calculations for the elements of the fifth and sixth columns of the Periodic Table including Mo, using a self-consistent augmented–plane-wave (APW) method. They also considered relativistic effects. The Fermi energy and the density of states were calculated by the linear tetrahedron method.[16–19]

It is clear from the foregoing remarks that, although there have been a number of band calculations of Mo, most of them have not gone beyond the calculations of the density of states and the interpretation of the Fermi surface data. The present work differs from previous studies in that we consider, in addition to the fundamental electronic structure, some related properties (x-ray form factors, Compton profile, and optical conductivity) which are, or can be, compared with experiment. In addition, we study the possible formation of a ferromagnetic state at expanded values of the lattice constant, and find that a moment may be expected to develop at a lattice constant of about 8.07 a.u. Although there have been many recent studies on possible ferromagnetic states of transition metals at large lattice constants,[1,2,20–34] calculations of this type for molybdenum have not been reported.

The outline of the paper is as follows. Section II contains a brief description of the band-structure calculation. We present, in Sec. III, the results of the band-structure calculation and the density of states; the calculated Fermi-surface cross sections are discussed in Sec. IV; the results of x-ray form factors and the Compton profile are given in Sec. V; we report the computation of the optical conductivity in Sec. VI; and in Sec. VII, we discuss the possibility of a ferromagnetically ordered state for expanded values of the lattice constant in Mo.

II. PROCEDURE

We employ a linear combination of atomic orbitals (LCAO) method, within the framework of the local-density approximation, in which the wave function is expanded in a set of Gaussian orbitals (LCGO).[3] This method does not make any shape approximation to charge densities or potentials. The details of this procedure are described in Ref. 3. We present below a brief description of some essential features of the present calculation.

The exchange-correlation potential used has the von Barth–Hedin form,[35] but with parameters given by Rajagopal, Singhal, and Kimball.[36]

The Gaussian-orbital basis is chosen from Ref. 37, and contains 16 *s* functions, 12 *p* functions, 8 *d* functions, and 1 *f* function; they are given in Table I. It may be noted

TABLE I. Orbital exponents of the Gaussian basis set.

1*s*	564 811.58
2*s*	84 340.172
3*s*	19 223.887
4*s*	5640.427
5*s*	1935.0108
6*s*	736.037 01
7*s*	304.546 61
8*s*	134.491 52
9*s*	50.361 75
10*s*	22.461 279
11*s*	7.711 217
12*s*	3.926 3438
13*s*	1.828 7531
14*s*	0.891 389 77
15*s*	0.394 964 69
16*s*	0.085 897 748
1*p*	4706.3308
2*p*	1104.2933
3*p*	361.171 22
4*p*	139.142 98
5*p*	58.356 511
6*p*	25.821 389
7*p*	10.718 475
8*p*	4.773 2916
9*p*	2.026 2457
10*p*	0.887 646 41
11*p*	0.342 082 79
12*p*	0.088
1*d*	172.7583
2*d*	51.005 487
3*d*	19.267 661
4*d*	7.922 9414
5*d*	3.378 5846
6*d*	1.329 3987
7*d*	0.495 317 99
8*d*	0.158 956 73
1*f*	0.8

that an extra p orbital and an f orbital were added to, and the most diffuse s orbital was deleted from, the original table.[37]

The value of the equilibrium lattice constant was estimated for $T=0$ K with the aid of measured thermal-expansion coefficients. This has been done because most Fermi-surface measurements are performed at low temperatures. The equilibrium lattice constant was found to be 5.942 84 a.u. This value was used to compute the quantities described in Secs. III–VI.

The calculations were carried out to self-consistency using 55 points in the $\frac{1}{48}$th (irreducible) part of the Brillouin zone. The final bands were generated at 506 points, and related properties were calculated with this grid. Relativistic effects were not included.

III. BAND STRUCTURE AND DENSITY OF STATES

The self-consistent band structure of bcc molybdenum obtained following the procedure described in the preceding section is plotted in Fig. 1. We have given the energies at selected symmetry points relative to the Fermi energy in Table II(a), together with the corresponding results obtained by five different methods, three of which are self-consistent methods. There is overall agreement among these results. In Table II(b), we give a brief summary of band calculations, along with selected band parameters. In the bcc lattice Γ and H are convenient points to use for discussing s-d– and d-band widths. The s-d– band width which is given by the H'_{25}-Γ_1 separation is found to be 0.761 Ry, which compares well with the average value 0.747 Ry of the other reported calculations. The H'_{25}-H_{12} separation measures the d-band width, and our value for this quantity is 0.693 Ry. This also compares very well with other reported values, especially with those which are obtained by APW methods.[6,15] The width of the occupied portion of the s-d band, E_F-$\varepsilon(\Gamma_1)$, is found to be 6.47 eV which is in reasonable agreement with the photoemission result of Kress and Lapeyre[38] who found it to be about 6 eV. The width of the occupied portion of the d band [E_F-$\varepsilon(H_{12})$] is found to be 5.55 eV which is in overall consistency with other calculations. It may be interesting to note that the widths of both the occupied portion and the total d band are larger than the corresponding values [E_F-$\varepsilon(H_{12})$=4.20 eV, and $\varepsilon(H'_{25})$-$\varepsilon(H_{12})$=6.53 eV] of its 3d counterpart, chromium,[39] obtained using the same procedures as employed here. d bands in the 3d elements are normally narrower than those of their 4d counterparts.

As in the cases of niobium and rhodium that we have discussed previously[1,2] there is reasonable general agreement between the results of different calculations as seen in Tables II(a) and II(b), even though the computational methods are quite different. In particular, the energies obtained in the self-consistent calculations (Refs. 13–15, and the present) agree for many (but by no means all) levels within roughly 0.2 eV. It is difficult to find a clear pattern in the differences. There is, apparently, a tendency for the pseudopotential calculation of Ref. 14 to give a more compressed band with excited states lower in energy than the others. One expects and finds that the inclusion of relativistic effects depresses the energy of the s-like state Γ_1 at the bottom of the band, and it is somewhat surprising not to find evidence of this for other s-like states (P_1,N_1).

The density of states was calculated by using the linear tetrahedron method[16–19] using 506 points and is plotted in Fig. 2. There are three main structures below the Fermi energy and two peaks above the Fermi energy. The peak positions in our plot are at −3.92, −3.02, −1.69, 1.62, and 2.24 eV, respectively, from the Fermi energy. In Table III(a), we have compared these positions with those obtained by some other calculations[6,13,14] and from photoemission experiments.[38,40] There is also good agreement between our positions and those obtained by other self-consistent calculations.[13,14]

The density of states at the Fermi energy was found to be 8.76 states atom^{-1} Ry^{-1}. This is in excellent agreement with other reported values [Table II(b)]. The electronic specific-heat coefficient γ_{band} was found to be

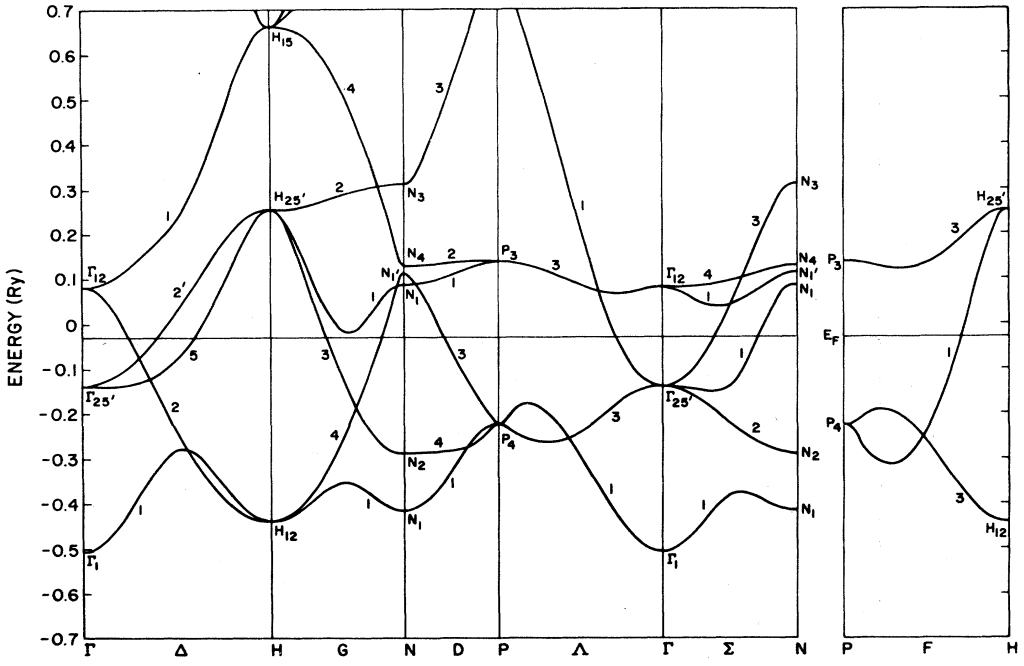

FIG. 1. Energy bands of bcc molybdenum.

3.6×10^{-4} cal/mol K^2. There are a number of measurements of this quantity.[41–46] We list them together with our results in Table III(b). They range between 4.8×10^{-4} and 5.26×10^{-4} cal/mol K^2. This suggests that, on an average, the experimental value is about 1.4 times that of the theoretical value, and this enhancement is presumably due primarily to the electron-phonon interaction. This is in fair agreement with the electron-phonon enhancement parameter 1.41 found from McMillan's theory.[47]

IV. FERMI SURFACE

The Fermi surface of molybdenum has been studied experimentally by the de Haas–van Alphen (dHvA) effect,[48–51] radio frequency size effect (RFSE),[52,53] magnetoacoustic geometric resonance effect,[54,55] and cyclotron resonance.[56] One of the distinguishing characteristics of molybdenum is the multiplicity of its Fermi-surface sheets. Bands 3–5 contribute to the Fermi surface, and there are four sheets. We discuss them below in the order of increasing number of carriers. The largest

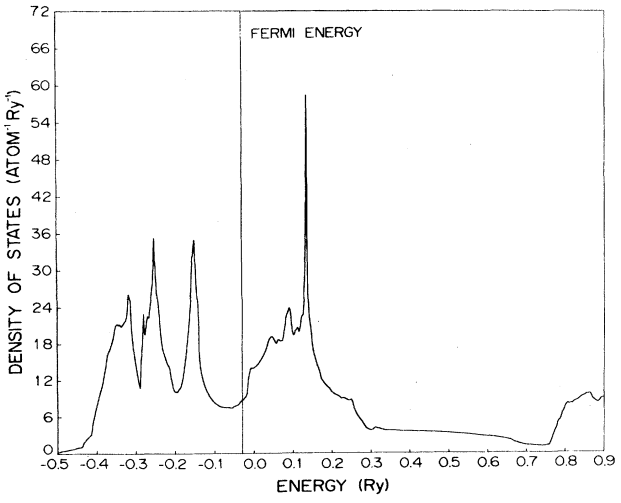

FIG. 2. Density of states of bcc molybdenum.

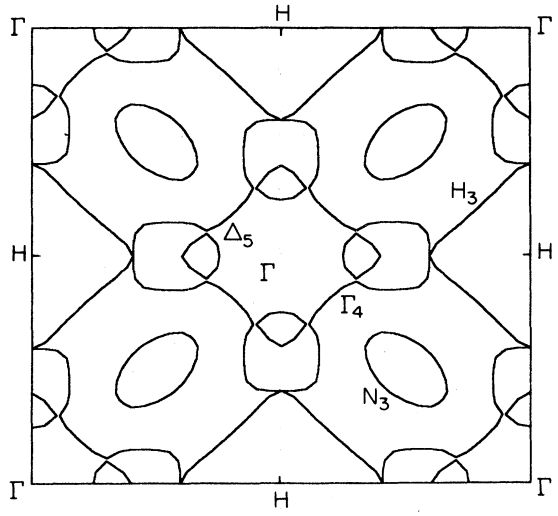

FIG. 3. Cross sections of the molybdenum Fermi surface in a (100) plane.

surface (Γ_4), which arises from the fourth band, is the electron jack centered at the Γ point of the Brillouin zone. The next largest surface (H_3) is the third-band hole octahedron at H. In addition, the third band also contributes six nearly ellipsoidal hole surfaces (N_3) at N. The smallest surfaces (Δ_5) are the six fifth-band electron lenses located at the Δ line. These Fermi-surface cross sections, which are labeled in Figs. 3 and 4, are drawn in planes (100) and (110). We have calculated the extremal areas of these cross sections, and as can be seen from Table IV, there is good agreement between our values and the experimental results,[51] as well as with the results of Ref. 10. It may be noted that a jack-octahedron separation is predicted by the experiments.[52,53] However, Figs. 3 and 4 do not show such separations because our calculation is nonrelativistic. The spin-orbit interaction in Mo produces separations between these pairs of surfaces.

V. X-RAY FORM FACTORS AND COMPTON PROFILES

A. X-ray form factors

The x-ray form factors are given by the expression

$$\rho(\mathbf{K})=\int \rho(\mathbf{r})e^{i\mathbf{K}\cdot\mathbf{r}}d^3r\ , \tag{5.1}$$

where the integration is over the whole crystal and ρ is normalized so that

$$\rho(0)=n_e \tag{5.2}$$

in which n_e is the number of electrons in the unit cell.

TABLE II. (a) Selected symmetry point energies (in eV) relative to the Fermi energy. The abbreviations relative to exchange-correlation potentials are as follows: KS (Kohn and Sham); SSTL (Singwi, Sjölander, Tosi, and Land); HL (Hedin and Lundqvist); and VBH-RSK (von Barth and Hedin, as parametrized by Rajagopal, Singhal, and Kimball). The abbreviations relative to methods are as follows: APW (augmented plane wave); KKR (Korringa-Kohn-Rostoker); NLP (non local pseudopotential); LCGO (linear combination of Gaussian orbitals); NSC (non-self-consistent); SC (self-consistent); and Rel (relativistic). (b) Comparison of band calculations. Energy differences are in Rydbergs.

(a)

	Ref. 6	Ref. 8	Ref. 13	Ref. 14	Ref. 15		Present
Lattice constant (a.u.)	5.947 83	5.9467	5.89	5.9584	5.953 48		5.942 84
Exchange-correlation potential	Slater	Renormalized atom	KS	KS and SSTL	HL and $X\alpha$		VBH-RSK
Method of calc.	APW-NSC	Renormalized atom—NSC	KKR-SC	NLP-SC	APW-SC Rel.	APW-SC Nonrel.	LCGO-SC
$\varepsilon(\Gamma_1)$	−6.64	−5.92	−6.50	−5.67	−7.3	−6.4	−6.47
$\varepsilon(\Gamma'_{25})$	−1.09	−1.49	−1.41	−1.52	−1.29	−1.36	−1.47
$\varepsilon(\Gamma_{12})$	1.46	1.37	1.34	1.51	1.47	1.32	1.52
$\varepsilon(H_{12})$	−5.49	−6.24	−5.93	−5.21	−5.69	−5.67	−5.55
$\varepsilon(H'_{25})$	3.87	4.16		3.21	3.91	3.71	3.88
$\varepsilon(H_{15})$	9.51			9.21	9.16	9.59	9.43
$\varepsilon(N_1)$	−5.06	−5.52	−5.40	−5.42	−5.40	−5.20	−5.23
$\varepsilon(N_2)$	−3.11	−3.71	−3.54	−3.61	−3.34	−3.38	−3.51
$\varepsilon(N_1)$	1.67	1.69		1.68			1.60
$\varepsilon(N'_1)$	1.66	2.42	1.58	1.36	1.49	1.94	1.96
$\varepsilon(N_4)$	2.18	2.27		1.68	2.16	2.00	2.16
$\varepsilon(N_3)$	4.58	5.06		3.63	4.69	4.47	4.64
$\varepsilon(N_1)$	11.85			9.41			12.20
$\varepsilon(P_4)$	−2.44	−2.62	−2.6	−2.88	−2.62	−2.54	−2.61
$\varepsilon(P_3)$	2.29	2.35		2.12	2.29	2.12	2.28
$\varepsilon(P_1)$	10.81			9.5	9.65	10.83	10.7

(b)

$\varepsilon(H'_{25})$-$\varepsilon(\Gamma_1)$	0.772	0.741		0.652	0.826	0.744	0.761
$\varepsilon(H'_{25})$-$\varepsilon(H_{12})$	0.688	0.764		0.619	0.706	0.690	0.693
$\varepsilon(N'_1)$-$\varepsilon(\Gamma_1)$	0.610	0.613	0.594	0.516	0.648	0.613	0.619
E_F-$\varepsilon(H_{12})$	0.403	0.458	0.436	0.383	0.418	0.417	0.408
E_F-$\varepsilon(\Gamma_1)$	0.488	0.435	0.477	0.416	0.538	0.470	0.475
$N(\varepsilon_F)$ (State/Ry/atom)	8.24		8.84	8.57	7.99	9.19	8.76

TABLE III. (a) Calculated and observed structures in the density of states of Mo, relative to the Fermi energy (in eV). (b) Electronic specific-heat coefficient γ_{band} (10^{-4} cal/mol K^2).

(a)

				Photoemission	
Ref. 6	Ref. 13	Ref. 14	Present	Ref. 38	Ref. 40
−4.28	−3.9	−3.96	−3.92	−3.9	−3.6
−2.92	−3.1	−2.92	−3.02		
−1.56	−1.6	−1.63	−1.64	−1.6	−1.6
1.50	1.6	1.61	1.62	1.0	
2.45		2.10	2.24	2.0	

(b)

Present work	3.6
Horowitz and Daunt (Ref. 41)	5.1±0.4
White and Woods (Ref. 42)	5.24
Shimizu, Takahashi, and Katsuki (Ref. 43)	5.05–5.25
Handbook Chem. Phys. (Ref. 44)	5.21
Hultgren *et al.* (Ref. 45)	5.26
S. A. Nemononov (Ref. 46)	4.8–5.1

The advantage of using the LCGO method is that one can obtain $\rho(\mathbf{K})$ directly from the band-structure calculations in terms of quantities called generalized overlap integrals,[3] and without additional labor.

We list our calculated x-ray form factors in Table V. The form factors for the atom are calculated from our starting charge densities, while those for the solid are obtained self-consistently. A comparison of these two sets of data reveal, as expected, that the form factors in bulk molybdenum differ only slightly from those of the free atom, thereby indicating that the overall electron distribution in the solid is close to that of the free atom. This statement, however, does not mean that the outermost or valence electrons are not redistributed in forming the solid; it means only that x-ray reflection intensities are represented well by the free-atom values of the form factors, and are not very sensitive to small redistributions of the electrons. Unfortunately, to our knowledge, there are no experimental results or previous theoretical calculations of the form factors.

We have also listed the angular anisotropies in the same table which define the ratio of the form factors for wave vectors $\mathbf{K}$ of the same magnitude, but different orientations such as (3,3,0) and (4,1,1); and (4.3,1) and (5,1,0).

B. Compton profile

An analysis of the Compton profile is important since it is sensitive to the state of the valence electrons of the solid. Since the revival of the Compton scattering technique about two decades ago, a great deal of work has been done on the Compton profile of solids. Experimental innovations such as the use of energy dispersive detectors and high-energy γ-ray sources have extended the application of this probe to heavier solids such as transition metals. Much of the earlier work on transition metals involved polycrystalline samples, whereas recently measurements have been carried out using single crystals. An extensive review of these data are given in Ref. 57.

We report in this work a computation of the Compton profile and its anisotropy in molybdenum. We have con-

TABLE IV. Calculated extremal areas of Fermi-surface cross sections (in a.u.).

Sheet	Planes	Koelling *et al.* Ref. 10	Present	Exp (Ref. 51)
Γ_4 (jack)	(100)	0.6282	0.6170	0.6174
	(110)	0.4313	0.4289	0.4223
H_3 (octahedron)	(100)	0.4110	0.393	0.4023
	(110)	0.3085	0.3089	0.3031
N_3 (ellipsoid)	(100)	0.0685	0.071	0.060
	(110)	0.0804	0.0798	0.0703
	(110)	0.1166	0.1205	0.0974
Δ_5	(100)		0.029	
	(110)	0.0170	0.0189	0.0137

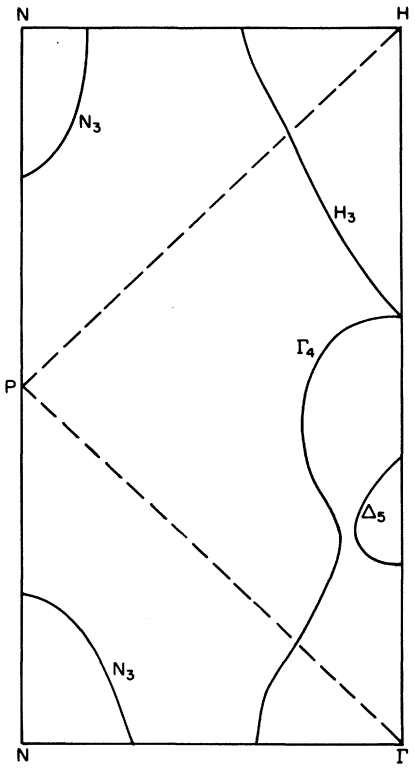

FIG. 4. Cross sections of the molybdenum Fermi surface in a (110) plane.

sidered only the valence-electron $(4d+5s)$ contribution to the Compton profile. We have not calculated the core contributions because a Hartree-Fock contribution of core electrons for the free atom is already available in the literature.[58] Since core electrons do not differ appreciably in the solid from those in the free atom, a free-atom core contribution would suffice to account for the total Compton profile.

TABLE V. X-ray form factors of molybdenum.

h	k	l	Atom	Solid
0	0	0	42.003	42.003
1	1	0	32.296	31.587
2	0	0	28.054	27.486
2	1	1	25.388	24.984
2	2	0	23.497	23.114
3	1	0	22.055	21.619
2	2	2	20.891	20.583
3	2	1	19.907	19.599
4	0	0	19.049	18.702
3	3	0	18.282	18.053
4	1	1	18.282	18.013
4	2	0	17.585	17.374
3	3	2	16.945	16.806
4	2	2	16.352	16.231
4	3	1	15.799	15.704
5	1	0	15.799	15.67
5	2	1	14.796	14.727
		Angular anisotropies		
$I(330)/I(411)$			1.0022	
$I(431)/I(510)$			1.0022	

TABLE VI. Calculated Compton-profile function in the [100], [110], and [111] directions together with the directional average profile.

q	$J_{[100]}(q)$	$J_{[110]}(q)$	$J_{[111]}(q)$	$J_{av}(q)$
0.0	2.370	2.589	2.827	2.588
0.1	2.373	2.580	2.772	2.570
0.2	2.313	2.505	2.638	2.485
0.3	2.296	2.388	2.395	2.364
0.4	2.244	2.264	2.190	2.239
0.5	2.171	2.109	1.987	2.095
0.6	2.101	1.975	1.874	1.985
0.7	2.018	1.863	1.788	1.888
0.8	1.856	1.764	1.757	1.789
0.9	1.712	1.635	1.682	1.669
1.0	1.548	1.453	1.483	1.488
1.1	1.300	1.259	1.154	1.244
1.2	1.058	1.077	0.854	1.014
1.3	0.887	0.866	0.761	0.845
1.4	0.784	0.677	0.795	0.738
1.5	0.576	0.556	0.716	0.603
1.6	0.417	0.460	0.514	0.461
1.7	0.319	0.376	0.369	0.358
1.8	0.279	0.304	0.299	0.295
1.9	0.252	0.269	0.255	0.261
2.0	0.243	0.238	0.221	0.235
2.1	0.228	0.210	0.202	0.213
2.2	0.201	0.186	0.191	0.192
2.3	0.172	0.168	0.164	0.168
2.4	0.154	0.146	0.131	0.145
2.5	0.125	0.122	0.122	0.122
2.6	0.089	0.103	0.123	0.104
2.7	0.068	0.086	0.106	0.086
2.8	0.057	0.069	0.071	0.066
2.9	0.050	0.057	0.050	0.053
3.0	0.044	0.049	0.040	0.045
3.1	0.042	0.042	0.035	0.040
3.2	0.037	0.036	0.032	0.035
3.3	0.032	0.032	0.030	0.031
3.4	0.027	0.028	0.030	0.029
3.5	0.025	0.025	0.029	0.026
3.6	0.022	0.022	0.023	0.022
3.7	0.020	0.020	0.020	0.020
3.8	0.018	0.018	0.019	0.019
3.9	0.017	0.017	0.018	0.017
4.0	0.015	0.016	0.017	0.016
4.1	0.015	0.015	0.015	0.015
4.2	0.014	0.014	0.013	0.014
4.3	0.014	0.013	0.013	0.013
4.4	0.013	0.013	0.013	0.013
4.5	0.014	0.013	0.013	0.013
4.6	0.014	0.014	0.013	0.013
4.7	0.013	0.012	0.012	0.012
4.8	0.012	0.011	0.009	0.011
4.9	0.011	0.011	0.008	0.011
5.0	0.011	0.011	0.010	0.011

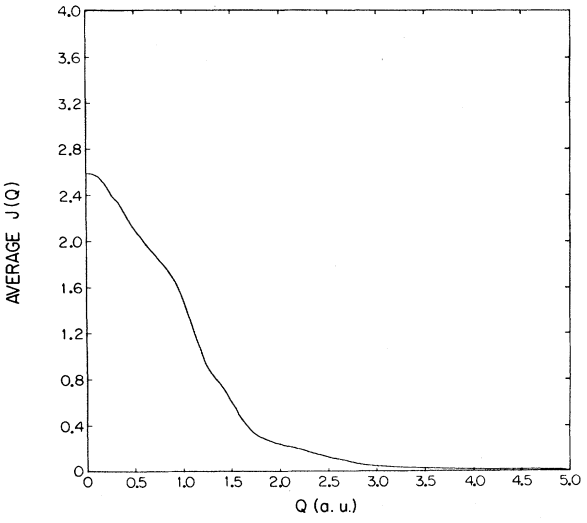

FIG. 5. Spherically averaged Compton profile of molybdenum.

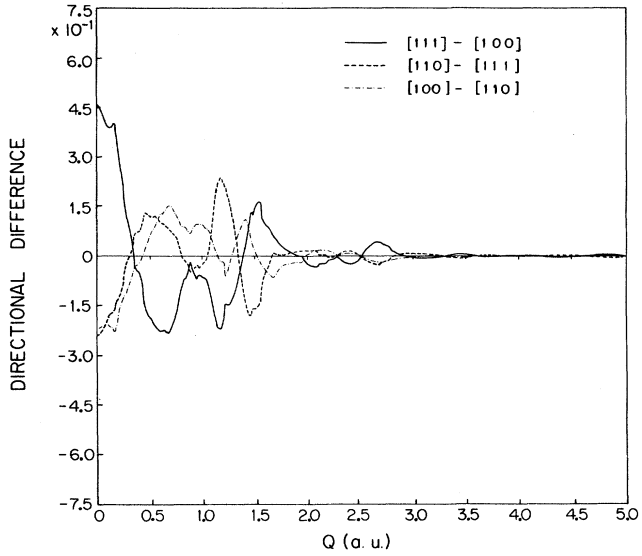

FIG. 6. Anisotropy of calculated Compton profile of molybdenum.

The Compton profile of the valence electrons was computed using the expression

$$J_{\hat{\mathbf{k}}}(q)=\frac{\Omega}{(2\pi)^3}\int d^3p\,\rho(\mathbf{p})\delta(q-\mathbf{p}\cdot\mathbf{k})\ , \tag{5.3}$$

where ρ is the momentum distribution function, $\hat{\mathbf{k}}$ is a unit vector along $\mathbf{k}$, Ω is the volume of the unit cell,

$$q=\frac{m\omega}{|\mathbf{k}|}-\tfrac{1}{2}|\mathbf{k}|\ , \tag{5.4}$$

and $\hbar\omega$ is the energy transferred to the electron after a Compton scattering event has occurred. The momentum density requires a summation over all occupied states. At $T=0$ K, this can be written as

$$\rho(\mathbf{p})=\sum_{n,\mathbf{k}}\Theta(E_F-E_n(\mathbf{k}))|\psi_n(\mathbf{k},\mathbf{p})|^2\ , \tag{5.5}$$

where E_F is the Fermi energy, $E_n(\mathbf{k})$ is the energy of a state, Θ is the unit step function, and $\psi_n(\mathbf{k},\mathbf{p})$ is the momentum-space Bloch function which is related to the position-space Bloch function by Fourier transformation.

The directional profiles were calculated using 506 points in the $\frac{1}{48}$th part of the Brillouin zone. The Compton profiles $J_{\hat{\mathbf{k}}}(q)$ along the [100], [110], and [111] directions together with the spherically averaged profile for each value of q ranging from 0 to 5 a.u. are given in Table VI. The spherically averaged profile is also plotted in Fig. 5. Differences of the Compton profile with respect to directions of the momentum transfer are shown in Fig. 6. Apparently, at present, there are no experimental results for molybdenum. It may, however, be noted that there have been some positron annihilation measurements[59,60] on molybdenum, and the resulting data have been analyzed by an independent particle model using APW techniques.[60] Since electron-positron correlation is important in the interpretation of annihilation measurements, a quantitative comparison between the Compton profile and the annihilation measurements is not possible. However, the Compton-profile results show the same qualitative features.

VI. OPTICAL CONDUCTIVITY

The study of the optical conductivity of metals is of interest in the sense that it provides quantitative information on the structure of energy bands. The optical conductivity of Mo has been studied experimentally by several groups.[61–63] Koelling *et al.*[64] have calculated the interband contribution to the optical conductivity of molybdenum in the range of 0 to 5.5 eV using a constant matrix-element approximation. They have used the result of a relativistic, non-self-consistent APW band-structure calculation for this purpose. Similar approximations have been made by Picket and Allen,[65] who calculated the imaginary part of the dielectric function of Mo using the results of an APW band-structure calculation. Since momentum matrix elements occurring in the expression of the optical conductivity determine the strength of optical transitions, the constant matrix-element approximation may be a severe one.

We have, therefore, calculated the frequency-dependent optical conductivity using the standard formula[66]

$$\sigma(\omega)=\frac{2\pi e^2}{3m^2\omega}\sum_{l,n}\int\frac{d^3k}{(2\pi)^3}|\langle l\mathbf{k}|\mathbf{p}|n\mathbf{k}\rangle|^2 f_l(\mathbf{k})[1-f_n(\mathbf{k})]\delta(E_n(\mathbf{k})-E_l(\mathbf{k})-\hbar\omega)\ , \tag{6.1}$$

where $f_l(\mathbf{k})$ and $f_n(\mathbf{k})$ are the Fermi distribution functions for bands l and n, respectively, and the remaining notation is conventional. The use of a Gaussian basis set facilitates the evaluation of the momentum matrix elements analytically, thus enabling one to retain the $\mathbf{k}$ dependence of these quantities. The $\mathbf{k}$-space integration was performed numerically by the linear tetrahedron method using 506 points.

The interband optical conductivity is plotted in Fig. 7(a). The major structure (peaks) occur at 2.05, 3.95, and 6.81 eV. Since, in our computation, contributions from various bands were not separated out, it is not possible to make assignments of peaks to particular transitions with much certainty. However, positions of these structures are in reasonable agreement with the same in experiments,[61–63] within the range studied. Furthermore, observed structures are not as sharp as the calculated ones. The discrepancy may be due to the lifetime broadening effect and the intraband Drude contribution. The Drude parameters are taken from Ref. 67. The effect of lifetime broadening has also been included with a choice of 0.29 eV for the reciprocal lifetime. We have plotted the combined results of the intraband and interband conductivities in Fig. 7(b). As is seen in Fig. 7, the calculated results are in satisfactory agreement with experimental results[61,62] within the limits of experimental uncertainties.

VII. MAGNETIC TRANSITION

There has been increasing interest in the study of the volume dependence of the magnetic properties of transition metals. It has been predicted that with some increase in the lattice constant, nonmagnetic transition metals will undergo a transition to a magnetically ordered state. Systems that are magnetic under normal conditions should lose their order if the lattice constant is decreased sufficiently. There have been a number of theoretical calculations pertaining to these phenomena.[20–34] Andersen and co-workers[20–22] have studied the volume dependence of the magnetic moment of bcc, fcc, and hcp Fe, using local-spin-density (LSD) and atomic-sphere approximations (ASA). Similar calculations have been performed by Kubler,[23] employing the augmented-spherical-wave procedure, and by Bagayoko and Callaway[24] using the LCGO method and the program BNDPKG.[3] The latter method has been used extensively to investigate the onset of the ferromagnetic moment in a number of transition metals,[1,2,25–28] including several $4d$ metals. On the other hand, Moruzzi and co-workers[29–31] have studied magnetic transitions in $3d$ metals by analyzing self-consistent total-energy band-structure calculations in the local-spin-density approximation utilizing a fixed-spin-moment procedure. In addition, several authors have used the general-potential linear augmented-plane-wave (LAPW) method to investigate the volume dependence of the magnetic moment of bcc and fcc Fe.[32–34] No investigation of molybdenum has been made to date.

We performed a spin-polarized band-structure calculation of molybdenum, using the LCGO method and the program BNDPKG, in the local-spin-density approximation. It has been found that bcc Mo is nonmagnetic (NM) at the equilibrium value of the lattice constant.

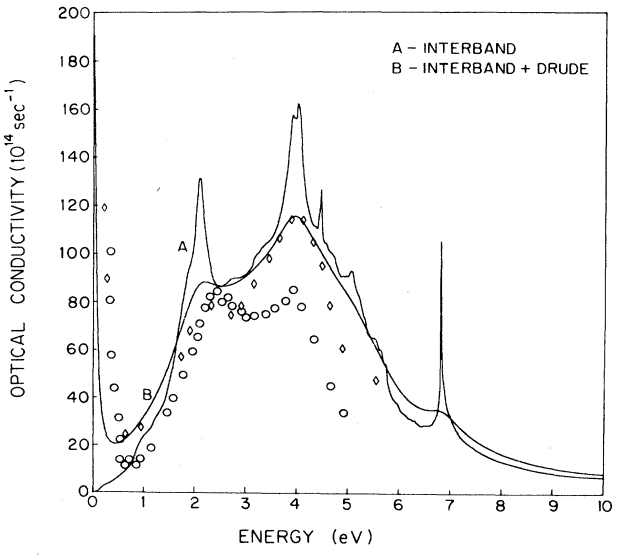

FIG. 7. Optical conductivity of molybdenum. Circles represent experimental points from Ref. 61 and diamonds represent experimental points from Ref. 62.

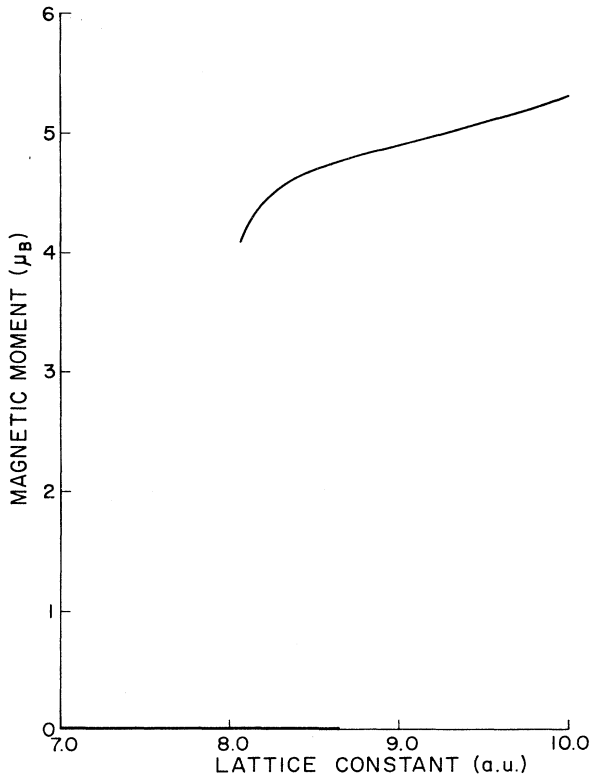

FIG. 8. Ferromagnetic moment of bcc molybdenum vs lattice constant.

TABLE VII. Calculated ferromagnetic moments for different values of the lattice constant.

Lattice constant (a.u.)	Magnetic moment m_1/μ_B	m_2/μ_B
5.942 84–8.05	0	
8.06	0	4.091
8.07	0	4.1145
8.12	0	4.265
8.25	0	4.493
8.35	0	
8.45	0	
8.75	0	
9.0		4.894
9.5		5.097
10.0		5.322

However, with increase in the lattice constant, Mo shows the following behavior: the magnetic moment is zero up to $a=8.06$ a.u.; there is a double-moment region between $a=8.06$ and 8.65 a.u.; and, finally, there is a single-valued high-spin (HS) state beyond $a=8.65$ a.u. The transition from the NM to HS state occurs discontinuously somewhere in the double-moment region. We are unable to predict the exact point at which the transition occurs since we have not performed a total-energy calculation. The highest value of the lattice constant considered for the computation of the ferromagnetic moment is 10.00 a.u., at which the value of the moment is $5.32\mu_B$, where μ_B is the Bohr magneton. We have not gone beyond this value because our basis set may not be adequate to describe the behavior beyond. However, we expect that, as the lattice constant is further increased, the magnetic moment will acquire its free-atom value of $6.0\mu_B$ in the LSD limit.[13] These calculations do not consider the possibility of antiferromagnetic order and therefore we cannot make definite predictions of the magnetic order in the ground state. The results obtained in this section are given in Table VII and plotted in Fig. 8.

VIII. CONCLUSIONS

Self-consistent band calculations of bcc molybdenum have been made in the local-density approximation using the LCGO method. A modified form of the von Barth–Hedin exchange-correlation potential has been employed. There is reasonable agreement with the results of other calculations employing different methods. The density of states was calculated using the linear tetrahedron method, and also agrees well with previous calculations and photoemission data. The electronic specific heat calculated using the density of states at the Fermi energy is found to be about 1.4 times less than the average experimental value, which is consistent with the electron-phonon enhancement parameter obtained using McMillan's theory. The calculated extremal areas of Fermi-surface cross sections agree well with experiment, as well as with a previous theoretical calculation. We have made the first detailed analysis of the Compton profile and its anisotropies in Mo. The interband optical conductivity was calculated using the **k** dependence of the matrix elements. There is satisfactory agreement between our results, which also include the Drude intraband contribution, and the experimental results. Finally, a spin-polarized band-structure calculation has been performed to study the lattice-constant dependence of the ferromagnetic moment in bcc Mo. It has been found that bcc Mo undergoes a discontinuous nonmagnetic to high-spin transition inside a double-moment region.

ACKNOWLEDGMENTS

This work was supported in part by the National Science Foundation under Grants No. DMR-85-04259 and No. DMR-88-10249. One of us (A.R.J.) is thankful to the Council for International Exchange of Scholars (CIES), Washingon, D.C. for financial support under the Indo-U.S. program.

*Permanent address: Sardar Patel University, Vallabh Vidyanagar 388 120, Gujarat State, India.

†Permanent address: Berhampur University, Berhampur 760 007, Orissa, India.

[1]G. S. Tripathi, N. E. Brener, and J. Callaway, Phys. Rev. B **38**, 10 454 (1988).

[2]A. R. Jani, N. E. Brener, and J. Callaway, Phys. Rev. B **38**, 9425 (1988).

[3]C. S. Wang and J. Callaway, Comput. Phys. Commun. **14**, 327 (1978).

[4]N. W. Ashcroft and N. D. Mermin, *Solid State Physics* (Holt, Reinhart, and Winston, New York, 1976), p. 49.

[5]T. L. Loucks, Phys. Rev. **139**, A1181 (1965).

[6]I. Petroff and C. R. Viswanathan, Phys. Rev. B **4**, 799 (1971).

[7]L. Hodges, R. E. Watson, and H. Ehrenreich, Phys. Rev. B **5**, 3953 (1972).

[8]R. J. Iverson and L. Hodges, Phys. Rev. B **8**, 1429 (1973).

[9]I. I. Geguzin, I. Y. Nikiforov, and G. I. Alperovich, Sov. Phys.—Solid State **15**, 646 (1973).

[10]D. D. Koelling, F. M. Mueller, A. J. Arko, and J. B. Ketterson, Phys. Rev. **10**, 4889 (1974).

[11]R. C. Cinti, E. Al Khoury, B. K. Chakraverty, and N. E. Christensen, Phys. Rev. B **14**, 3296 (1976).

[12]G. I. Alperovich, I. I. Geguzin, A. V. Nikolskii, V. G. Kochetov, and I. Y. Nikiforov, Izv. Akad. Nauk SSSR, Ser. Fiz. **40**, 251 (1976).

[13]V. L. Moruzzi, J. F. Janak, and A. R. Williams, *Calculated Electronic Properties of Metals* (Pergamon, New York, 1978), p. 128.

[14]A. Zunger, G. P. Kerker, and M. L. Cohen, Phys. Rev. B **20**, 581 (1979).

[15]N. C. Bacalis, K. Blatharas, P. Thomaides, and D. A. Papaconstantopoulous, Phys. Rev. B **32**, 4849 (1985).

[16]O. Jepsen and O. K. Andersen, Solid State Commun. **9**, 1763 (1971).

[17]G. Lehman and M. Taut, Phys. Status Solidi **54**, 469 (1972).

[18]J. Rath and A. J. Freeman, Phys. Rev. B **11**, 2109 (1975).
[19]L. Kleinman, Phys. Rev. B **28**, 1139 (1983).
[20]J. Madsen and O. K. Andersen, in *Magnetism and Magnetic Materials,* edited by J. J. Becker, G. H. Lauder, and J. J. Phyne (AIP, New York, 1975), p. 327.
[21]U. K. Poulson, J. Kollar, and O. K. Andersen, J. Phys. F **6**, 241 (1976).
[22]O. K. Andersen, J. Madsen, U. K. Poulson, O. Jepsen, and J. Kollar, Physica **86-88B**, 249 (1977).
[23]J. Kubler, Phys. Lett. **81A**, 81 (1981).
[24]D. Bagayoko and J. Callaway, Phys. Rev. B **28**, 5419 (1983).
[25]J. L. Fry, Y. Z. Zhao, N. E. Brener, G. Fuster, and J. Callaway, Phys. Rev. B **36**, 868 (1987).
[26]G. Fuster, N. E. Brener, J. Callaway, J. L. Fry, Y. Z. Zhao, and D. A. Papaconstantopoulos, Phys. Rev. B **38**, 423 (1988).
[27]N. E. Brener, G. Fuster, J. Callaway, J. L. Fry, and Y. Z. Zhao, J. Appl. Phys. **63**, 4057 (1988).
[28]N. E. Brener, J. Callaway, G. Fuster, G. S. Tripathi, and A. R. Jani, J. Appl. Phys. **64**, 5601 (1988).
[29]V. L. Moruzzi, P. M. Marcus, K. Schwarz, and P. Mohn, Phys. Rev. B **34**, 1784 (1986).
[30]V. L. Moruzzi, P. M. Marcus, and P. C. Pattnaik, Phys. Rev. B **37**, 8003 (1988).
[31]V. L. Moruzzi and P. M. Marcus, Phys. Rev. B **38**, 1613 (1988).
[32]K. B. Hathaway, H. J. F. Jansen, and A. J. Freeman, Phys. Rev. B **31**, 7603 (1985); H. J. F. Jansen, K. B. Hathaway, and A. J. Freeman, *ibid.* **30**, 6177 (1984).
[33]C. S. Wang, B. M. Klein, and H. Krakauer, Phys. Rev. Lett. **54**, 1852 (1985).
[34]H. J. F. Jansen and S. S. Peng, Phys. Rev. B **37**, 2689 (1988).
[35]U. von Barth and L. Hedin, J. Phys. C **5**, 1629 (1972).
[36]A. K. Rajagopal, S. P. Singhal, and J. Kimball (unpublished), as quoted by A. K. Rajagopal, *Advances in Chemistry and Physics,* edited by G. I. Prigogine and S. A. Rice (Wiley, New York, 1979), Vol. 41, p. 59.
[37]R. Poirer, R. Kari, and I. G. Csizmadia, Phys. Sci. Data **34**, 9485 (1985).
[38]K. A. Kress and G. J. Lapeyre, *Title,* Nat. Bur. Stand. (U.S.) Spec. Publ. No. 323 (U.S. GPO, Washington, D.C., 1971), p. 209.
[39]D. G. Laurent, J. Callaway, J. L. Fry, and N. E. Brener, Phys. Rev. B **23**, 4977 (1981).
[40]D. E. Eastman, Solid State Commun. **1**, 1697 (1969).
[41]M. Horowitz and J. G. Daunt, Phys. Rev. **91**, 1099 (1953).
[42]G. K. White and S. B. Woods, Phil. Trans. R. Soc. London Ser. A **215**, 35 (1959).
[43]M. Shimizu, T. Takahashi, and A. Katsuki, J. Phys. Soc. Jpn. **17**, 1740 (1962).
[44]*Handbook of Chemistry and Physics,* edited by R. C. Weast (Chemical Rubber, Cleveland, Ohio, 1967), p. D.100.
[45]R. R. Hultgren, R. L. Orr, P. D. Andersen, and K. K. Kelley, *Selected Values of Thermodynamic Properties of Metals and Alloys* (Wiley, New York, 1963), p. 308.
[46]S. A. Nemononov, Fiz. Met. Metalloved. **19**, 550 (1972).
[47]W. McMillan, Phys. Rev. **167**, 331 (1968).
[48]G. B. Brandt and J. A. Rayne, Phys. Rev. **132**, 1945 (1963).
[49]D. M. Sparlin and J. A. Marcus, Phys. Rev. **144**, 848 (1966).
[50]G. Leaver and A. Myers, Philos. Mag. **19**, 465 (1969).
[51]J. Hoekstra and J. L. Stanford, Phys. Rev. B **8**, 1416 (1973).
[52]V. V. Boiko, V. A. Gasparov, and I. G. Gverdtsiteli, Zh. Eksp. Teor. Fiz. **56**, 489 (1969) [Sov. Phys.—JETP **29**, 269 (1969); V. V. Boiko and V. A. Gasparov, *ibid.* **61**, 1976 (1971) [*ibid.* **34**, 1054 (1972)].
[53]J. R. Cleveland and J. L. Stanford, Phys. Rev. B **4**, 311 (1971).
[54]C. K. Jones and J.A. Rayne, Phys. Lett. **8**, 155 (1964).
[55]P. A. Bezuglyi, S. E. Zherago, and V. I. Denisenko, Zh. Eksp. Teor. Fiz. **49**, 1457 (1965) [Sov. Phys.—JETP **22**, 1002 (1966)].
[56]R. Herrmann, Phys. Status Solidi **25**, 427 (1968); R. Herrmann and H. Krueger, *ibid.* **41**, 99 (1971).
[57]B. Williams, *Compton Scattering* (McGraw-Hill, New York, 1977), p. 159.
[58]F. Biggs, L. B. Mendelsohn, and J. B. Mann, At. Data Nucl. Data Tables **16**, 201 (1975).
[59]S. M. Kim and W. J. L. Buyers, Can. J. Phys. **50**, 1777 (1972).
[60]N. Shiotani, T. Okada, H. Sekizawa, S. Wakoh, and Y. Kubo, J. Phys. Soc. Jpn. **43**, 1229 (1977).
[61]M. M. Kirillova, G. A. Bolotin, and V. M. Mayevskiy, Phys. Met. Metalloved. **24**, 95 (1967).
[62]B. W. Veal and A. P. Paulikas, Phys. Rev. B **10**, 1280 (1974).
[63]E. S. Black, D. W. Lynch, and C. G. Olson, Phys Rev. B **16**, 2337 (1977).
[64]D. D. Koelling, F. M. Mueller, and B. W. Veal, Phys. Rev. B **10**, 1290 (1974).
[65]W. E. Pickett and P. B. Allen, Phys. Rev. B **11**, 3599 (1975).
[66]D. G. Laurent, J. Callaway, and C. S. Wang, Phys. Rev. B **20**, 1134 (1979).
[67]A. P. Lenham and D. M. Treherne, in *Optical Properties and Electronic Structure of Metals and Alloys,* edited by F. Abeles (North-Holland, Amsterdam, 1966), p. 196.